minerals

MDPI

Article

Spectral Characteristics, Rare Earth Elements, and Ore-Forming Fluid Constrains on the Origin of Fluorite Deposit in Nanlishu, Jilin Province, China

Xiaomeng Ye and Feng Bai *

School of Gemmology, China University of Geosciences, Beijing 100083, China
* Correspondence: baifeng@cugb.edu.cn

Abstract: Nanlishu fluorite has had an annual output of nearly 10,000 tons since its discovery and mining in 1987. At present, few studies have been undertaken on the genesis of the Nanlishu fluorite deposit. Microscopy, Fourier transform infrared (FTIR) spectroscopy, Raman microprobe spectroscopy, and ultraviolet–visible (UV–Vis) spectroscopy were used to study the mineral composition, mineral structure, and spectral characteristics, and fluid inclusion and rare earth element (REE) geochemistry studies were conducted to discuss the characteristics and evolution of the ore-forming fluids and the mineralization process. The Nanlishu fluorite ore rock is composed mainly of fluorite, with minor amounts of quartz, pyrite, and apatite, and trace amounts of calcite. The purple in the fluorite is caused by the Ca colloids. The homogenization temperatures of fluid inclusions in Nanlishu fluorite vary from 116 to 179 °C, while the salinity ranges from 0.35 to 4.03 wt% NaCl equiv, and the density varies from 0.90 to 1.00 g/cm^3. Ore-forming fluids were derived from heated meteoric water characterized by low temperature, low salinity, and low density. The total rare earth element (∑REE, excluding Y) content of the ore ranged from 8.072 to 27.230 ppm. The light/heavy REE ratio (LREE/HREE) varies from 0.971 to 1.513. The δEu value is 1.010–1.074 and the δCe value is 0.893–1.048. Compared with other deposits, the Nanlishu fluorite has lower ∑REE content, no obvious enrichment of LREEs or HREEs, and no anomalies in δEu and δCe. Water/rock reaction is the main mechanism for Nanlishu fluorite precipitation. The Nanlishu fluorite is a fault-controlled, low-temperature hydrothermal, fracture-filling deposit.

Keywords: Nanlishu; fluorite; spectral characteristics; fluid inclusions; ore-forming fluid

Citation: Ye, X.; Bai, F. Spectral Characteristics, Rare Earth Elements, and Ore-Forming Fluid Constrains on the Origin of Fluorite Deposit in Nanlishu, Jilin Province, China. *Minerals* **2022**, *12*, 1195. https://doi.org/10.3390/min12101195

Academic Editors: Helmut Cölfen and Oliver Oeckler

Received: 26 August 2022
Accepted: 16 September 2022
Published: 23 September 2022

1. Introduction

Fluorite, also known as fluorspar, is composed mainly of calcium fluoride (CaF_2), in which Ca can be replaced by the isomorphism of Y, U, Th, or Sr. It is commonly colorless, green, blue, purple, or pink, and is the mineral with the most color varieties in nature. Fluorite from many origins has been studied, and the main chromogenic mechanisms are color centers [1–4], rare earth element (REE) impurities [5–7], and Ca colloids [8–10].

The REEs in fluorite can represent the elemental composition of the ore-forming fluid and contain geochemical information about the mineralization process, which makes it possible to trace geological and geochemical processes [11–15]. Fluid inclusions, the direct samples of remaining ore-forming fluids, are the key to studying the physicochemical conditions of the ore-forming fluids and metallogenesis [16–21].

Nanlishu fluorite, the main mineral in the deposit, has had an annual output of nearly 10,000 tons since it entered production in 1987. It sells for a high price and the global supply of fluorite ore is tight. The economic benefits are considerable. At present, few studies have been undertaken on the genesis of the Nanlishu fluorite deposit. In combination with field observations, Liu believes that the Nanlishu fluorite ore-forming fluid is a late magmatic hydrothermal solution (intrusion of the quartz syenite porphyry) [22]. In China, however, fluorite in magmatic hydrothermal deposits is often associated with other main

minerals [23–29]. Only in deposits with meteoric water as the main ore-forming fluid, fluorite can be the main mineral [30–33].

In this work, microscopy, Fourier transform infrared (FTIR) spectroscopy, Raman microprobe spectroscopy, and ultraviolet-visible (UV-Vis) spectroscopy were used to study the mineral composition, mineral structure, and spectral characteristics, while fluid inclusion and REE geochemistry analyses were conducted to discuss the characteristics and evolution of the ore-forming fluids and the mineralization process.

2. Regional Geologic Background

Surface outcrops in the study area comprise the Carboniferous, Jurassic, and Quaternary strata (Figure 1). North–northwest trending Carboniferous strata are distributed in the northern and eastern parts of the mining area. The main lithologies are metamorphic sandstone, limestone, slate, siliceous rock, and tuff, which are closely related to mineralization and are the direct surrounding rock of the Nanlishu fluorite ore bodies. The Jurassic strata are located in the northwest of the mining area, unconformably overlying the Carboniferous strata, and the main lithologies are intermediate-felsic volcanic rocks. The Quaternary strata are mainly gravel, sand, and loam.

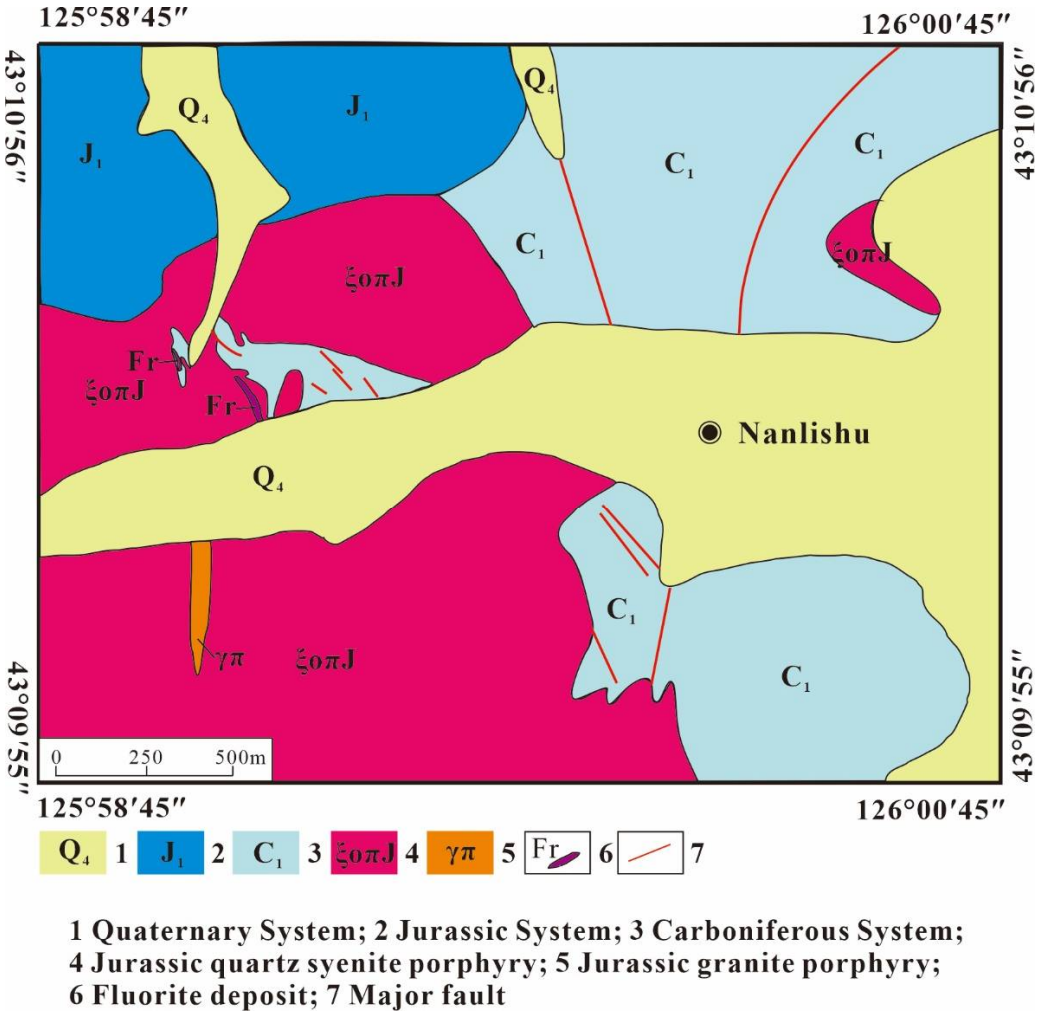

Figure 1. Geological map of the mining area of the Nanlishu fluorite deposit in Mingcheng Town, Panshi City (after Yan, 2019) [22].

The structure in the study area is complicated. Folds and faults are directly related to mineralization. The Carboniferous strata were affected by the early Indosinian tectonic movement and formed linear folds. The compressional torsional Lishugou fault is the

largest and traverses the whole area. Due to its influence, two sets of secondary faults were produced that are oriented north–east and north–west. The NW-trending faults are oriented at 320–340°; fluorite is mainly developed in this fault system. The NE-trending faults are small in scale, unstable in strikes, and have dip angles of 50–84°. In addition to these faults, NNE-trending faults and NW-trending compressive fracture belts are also developed in the area.

The intrusive magmatic rocks in the area are mainly Jurassic quartz syenite porphyry and granite porphyry veins. These crop out in a wide area. The quartz syenite porphyry intrudes into the Carboniferous and Jurassic strata, and the granite porphyry intrudes into the quartz syenite porphyry in the form of veins.

The parallel, vein-type, and lens-type ore bodies are controlled by the faults. The top of the ore bodies is tuff, which partially surrounds the ore bodies, while the bottom of the ore bodies is mainly quartz syenite porphyry. Other ore bodies are hosted in the interlayer fracture belt in limestone and argillaceous limestone. Tuff in direct contact with the ore bodies underwent silicification and pyritization [22].

3. Materials and Methods

The granular, massive Nanlishu fluorite ore is mainly purple in color, accompanied by gray and white. For this study, five samples were selected and used as the raw material (O1, O2, O3, O4, O5). O1, O2, and O3 are mainly composed of fluorite. O4 is filled with white vein-type quartz and O5 includes gray–green breccia (Figure 2). Parts with purple, gray, and white color were selected from each sample to prepare petrographic polished slices and thin sections. The polished slices and thin sections were observed and photographed using a BX51 polarized light microscope (PLM) at the Experimental Teaching Center of Jewelry and Mineral Materials, China University of Geosciences, Beijing.

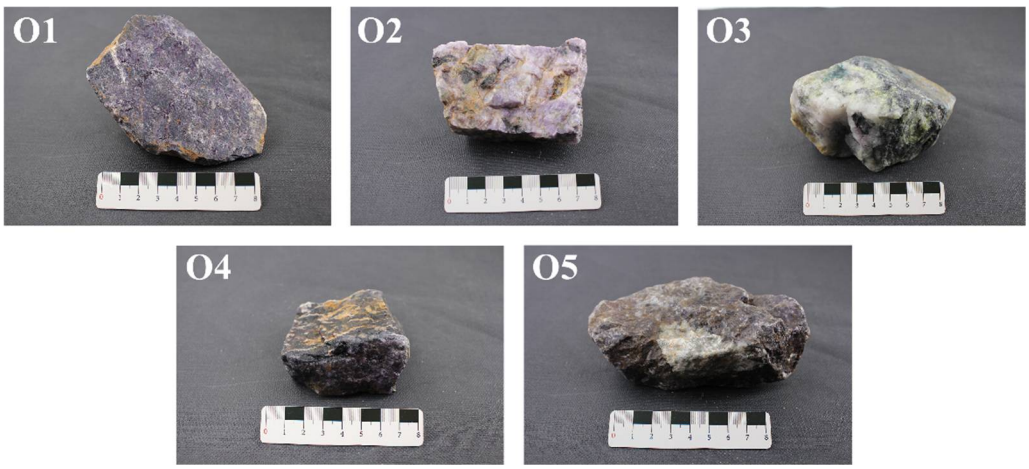

Figure 2. Selected samples of Nanlishu fluorite ore (marked in centimeters).

Fourier transform infrared (FTIR) spectra, Raman microprobe spectra, and UV–Vis spectra were acquired at the Experimental Teaching Center of Jewelry and Mineral Materials, China University of Geosciences, Beijing. The FTIR spectra for the five samples were recorded in transmission mode using a Bruker Tensor 27 FTIR spectrometer. The ore was ground into 200-mesh powder using an agate mortar, and the powder was mixed with KBr in a ratio of 1:150 and compressed into a tablet. The analytical conditions used for measurement included a resolution of 4 cm^{-1}, a scan range of 400–2000 cm^{-1}, and a run time of 30 s per scan.

Based on the PLM observations, petrographic thin sections corresponding to different color samples were selected and measured using a Horiba Scientific Raman microprobe spectrometer. Analysis conditions included an excitation wavelength of 532 nm, a scan

range of 100–1200 cm^{-1}, a resolution of 4 cm^{-1}, and a spot size of 5 μm; each spectrum was scanned three times for 5 s.

Each purple sample was polished and cut into square sections of 1 cm × 1 cm × 1 cm to further explore the origin of purple generation. The UV–Vis spectra were measured using a UV-3600 spectrophotometer with operating conditions of reflection mode, scanning range of 300–800 nm, a sampling interval of 0.5 s, and high-speed scan mode.

Microthermometry of fluid inclusions was performed using a Linkam MDSG 600 heating–freezing system attached to a ZEISS PLM at the State Key Laboratory of Geological Processes and Mineral Resources, China University of Geosciences, Beijing. The measurable temperature range was −100 to +398 °C. Most of the tests were kept at a rate of 5–30 °C/min, but the rate was controlled at 0.1–1 °C/min near the phase transition point. Concurrently, the fluid inclusion component analyses were measured using a Horiba Scientific Raman microprobe spectrometer. Analysis conditions included an excitation wavelength of 532 nm, a scan range of 100–5000 cm^{-1}, a resolution of 4 cm^{-1}, and a spot size of 1–5 μm; each spectrum was scanned three times for 5 s.

The rare earth elements were analyzed by the acid solution method [17]. The ore was ground into 200-mesh powder. Then, 25 mg of powder, 0.5 mL of nitric acid, and 1.5 mL of hydrofluoric acid were placed into the digestion vessel and heated at 220 °C for 24 h. After cooling, they were placed on an electric heating plate and evaporated at 165 °C. Next, 1 mL of nitric acid was added and evaporated twice. Then, 3 mL of nitric acid (50%) was added, and they were heated in the digestion vessel at 165 °C for 5 h. Finally, the capacity was determined to be 25 mL. The analysis of rare earth elements was acquired using an Agilent 7500a inductively coupled plasma mass spectrometer at the National Research Center for Geoanalysis, Beijing.

4. Results

4.1. Structure and Components

Figure 3 shows some microphotographs of polished slides of samples of fluorite from the Nanlishu deposit. O1 and O2 consisted mainly of fluorite, which was frequently filled with vein-type quartz (Figure 3a). The distribution of small particles of pyrite was uneven, forming colloidal aggregates in association with quartz (Figure 3b). Some hypidiomorphic–xenomorphic pyrite had grain sizes of approximately 5–20 μm in association with quartz (Figure 3c). There was xenomorphic granular apatite with grain sizes of approximately 5–10 μm in association with quartz along the edges of fluorite (Figure 3d). O3 was composed of only fractured fluorite with no quartz or other minerals, suggesting that the fluorite in O3 formed later than the fluorite in O1 and O2 (Figure 3e). O4 was composed of fluorite filled with quartz (Figure 3f).

Figure 4 shows some microphotographs of thin sections of samples of fluorite from the Nanlishu deposit. O1 and O2 consisted mainly of fluorite. In combination with the hand specimen observations, it was concluded that the fluorite formation in O1 and O2 can be divided into two stages: All early fluorite had more developed fractures, dark purple, small grains, and a massive appearance filled with quartz (Figure 4a,b). The late fluorite had light purple, white or gray, large grains, and crystallized along the crystallographic planes of the early fluorite. It was not filled with quartz (Figure 4c). O3 was composed of late, light-colored fluorite with purple stripes or corrugations and was not filled with quartz (Figure 4d). O4 was composed of the early fluorite and quartz, and the vein-type quartz included the early fluorite (Figure 4e). The breccia mineral in O5 was colorless and transparent, with obvious rhombic cleavage, which suggested that it was calcite (Figure 4f).

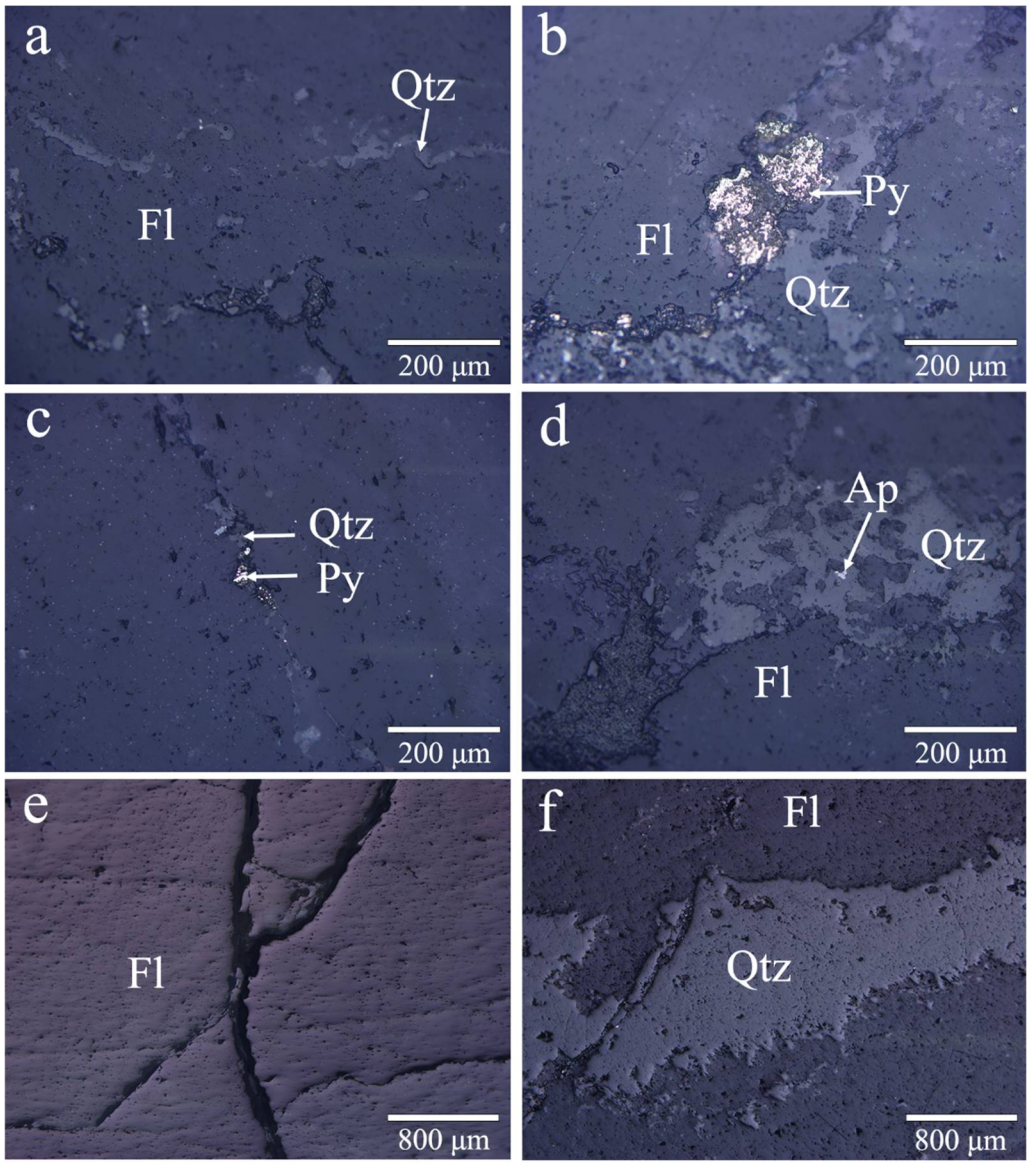

Figure 3. Mineral microstructure of the ore samples under reflected light. (**a**) Fluorite filled with vein-type quartz (O1); (**b**) colloidal pyrite in association with quartz (O1); (**c**) pyrite with grain sizes of approximately 5–20 μm (O2); (**d**) apatite in association with quartz (O1); (**e**) fluorite with developed fractures (O3); (**f**) coarse vein-type quartz (O4). Fl, fluorite; Qtz, quartz; Py, pyrite; Ap, apatite.

4.2. Spectroscopy

4.2.1. FTIR Spectra

The FTIR transmissive spectra for the samples are all quite similar, and the transmission peaks can be divided into three groups: (1) 1033–1020 cm^{-1}, (2) 1589–1637 cm^{-1}, and (3) 460–796 cm^{-1} (Figure 5a–d). The bands at 1033, 1039, 1083, and 1120 cm^{-1} and at 1593, 1595, 1620, and 1625 cm^{-1} are due to the CO_3^{2-} stretching modes [34]. There are small deviations in the FTIR bands for the different samples, which is caused by the CO_3^{2-} and other impurity ions. The bands at 460–796 cm^{-1} only appear in sample O4, which was filled with white vein-type quartz; therefore, these bands are related to the quartz. The band at 460 cm^{-1} is ascribed to the Si–O bending mode, and the bands at 692, 777, and 796 cm^{-1} are attributed to the Si–O symmetrical stretching mode [35–37].

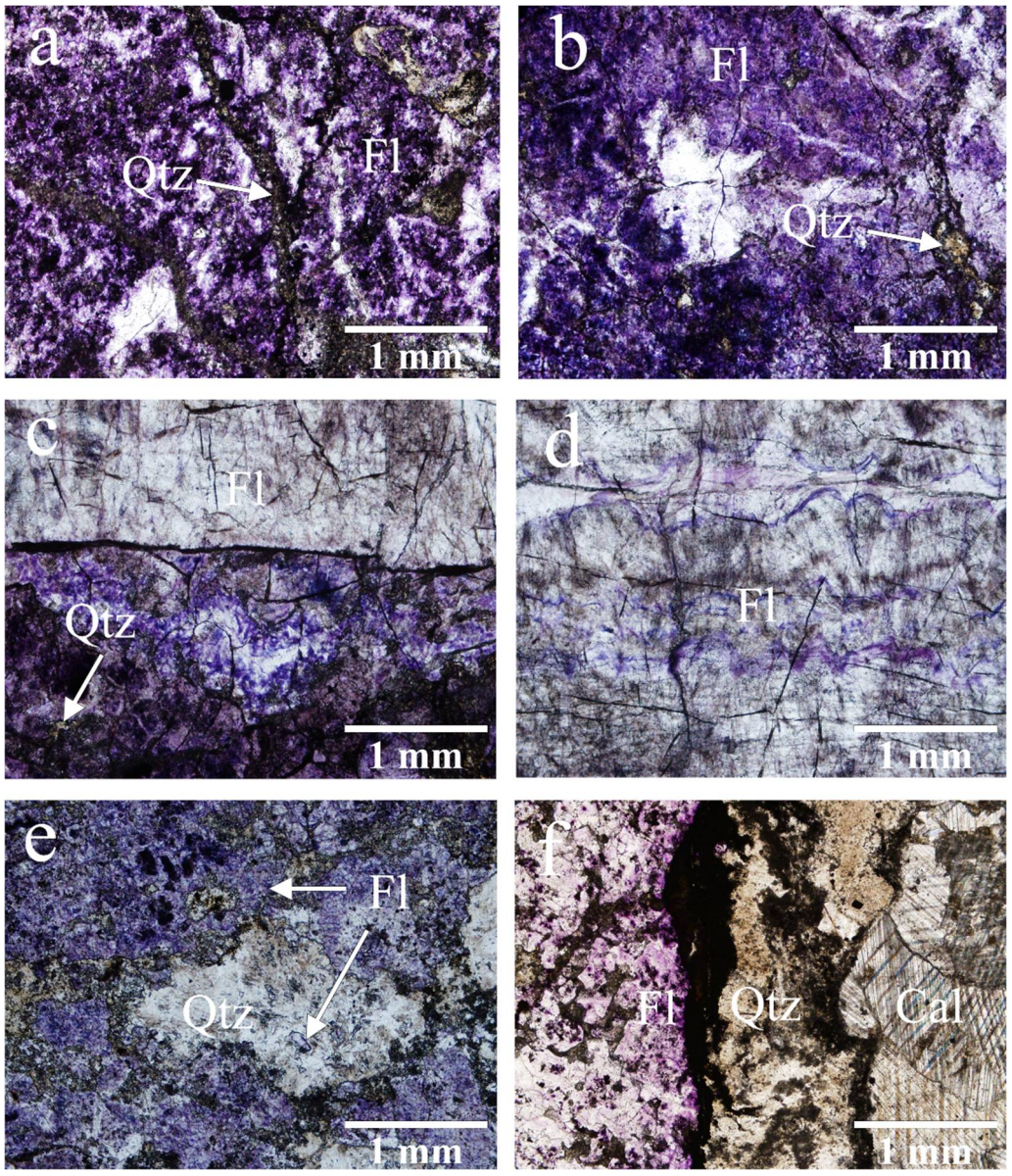

Figure 4. Mineral microstructures of the ore samples under transmitted light. (**a**,**b**) Vein-type quartz filled with early fluorite (O1 and O2, respectively); (**c**) late fluorite crystallized along the crystallographic planes of the early fluorite (O1); (**d**) late fluorite with purple stripes or corrugations (O3); (**e**) the vein-type quartz including the early fluorite (O4); (**f**) calcite with obvious rhombic cleavage (O5). Fl, fluorite; Qtz, quartz; Cal, calcite.

The main mineral of the ore is fluorite. The transmission peaks caused by the CO_3^{2-} stretching mode appear in all measured samples, indicating that the Nanlishu fluorite ore contains carbonate minerals. In combination with PLM observations, the carbonate mineral is calcite from the surrounding rock, which can provide the Ca required for fluorite mineralization. The strong bending and stretching Si–O bands are related to the quartz formed by hydrothermal solution deposition.

4.2.2. Raman Spectra

The only band ascribable to fluorite's ideal structure is positioned at 319 or 321 cm^{-1} (Figure 6a–d). The weak bands at 140, 142, 144, 227, and 282 cm^{-1} in O1, O2, O3, and O4 are assigned to the lattice modes [38–40]. Based on measurements of the petrographic thin sections at selected regions of interest, the Raman microprobe spectra for quartz, apatite,

pyrite, and calcite were also analyzed (Figure 7a–d). The assignments of the Raman shifts are listed in Table 1.

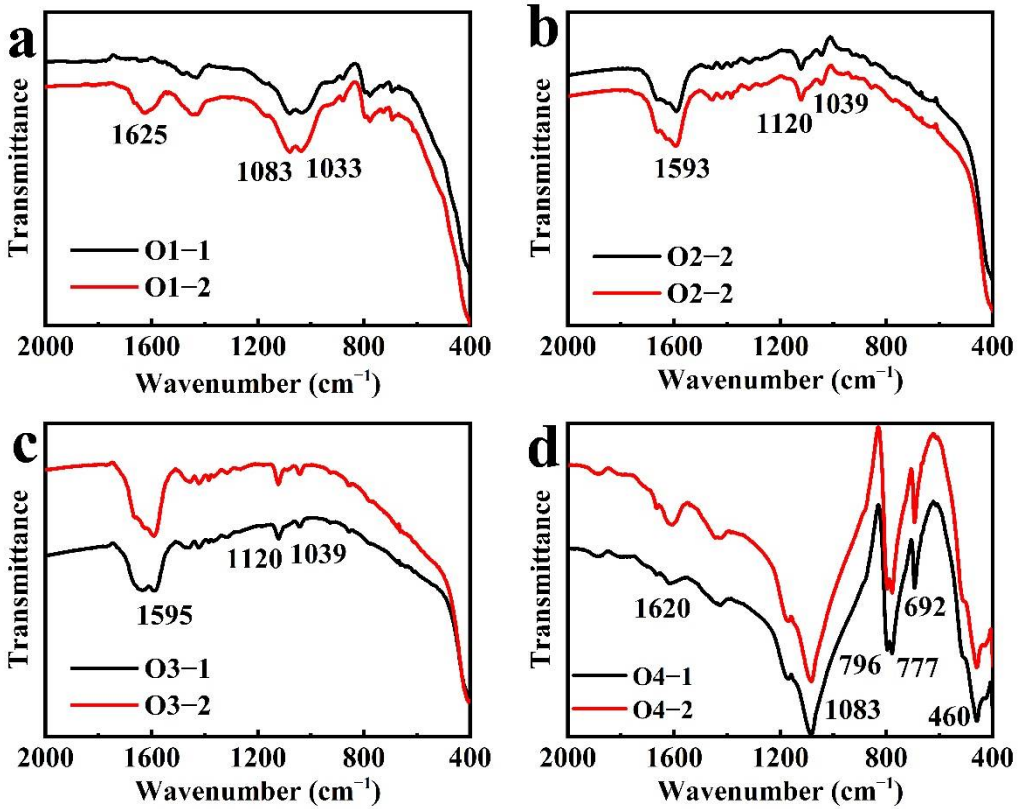

Figure 5. Fourier transform infrared FTIR spectra of the ore samples. (**a**) O1; (**b**) O2; (**c**) O3; (**d**) O4.

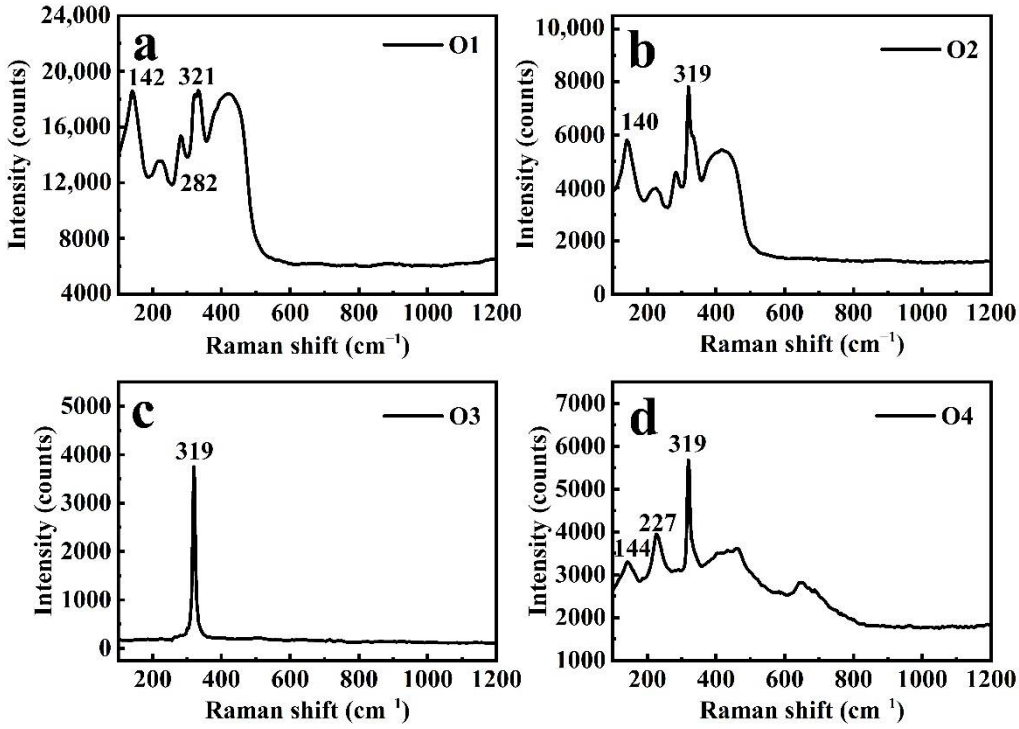

Figure 6. The Raman microprobe spectra for fluorite in the ore samples. (**a**) O1; (**b**) O2; (**c**) O3; (**d**) O4.

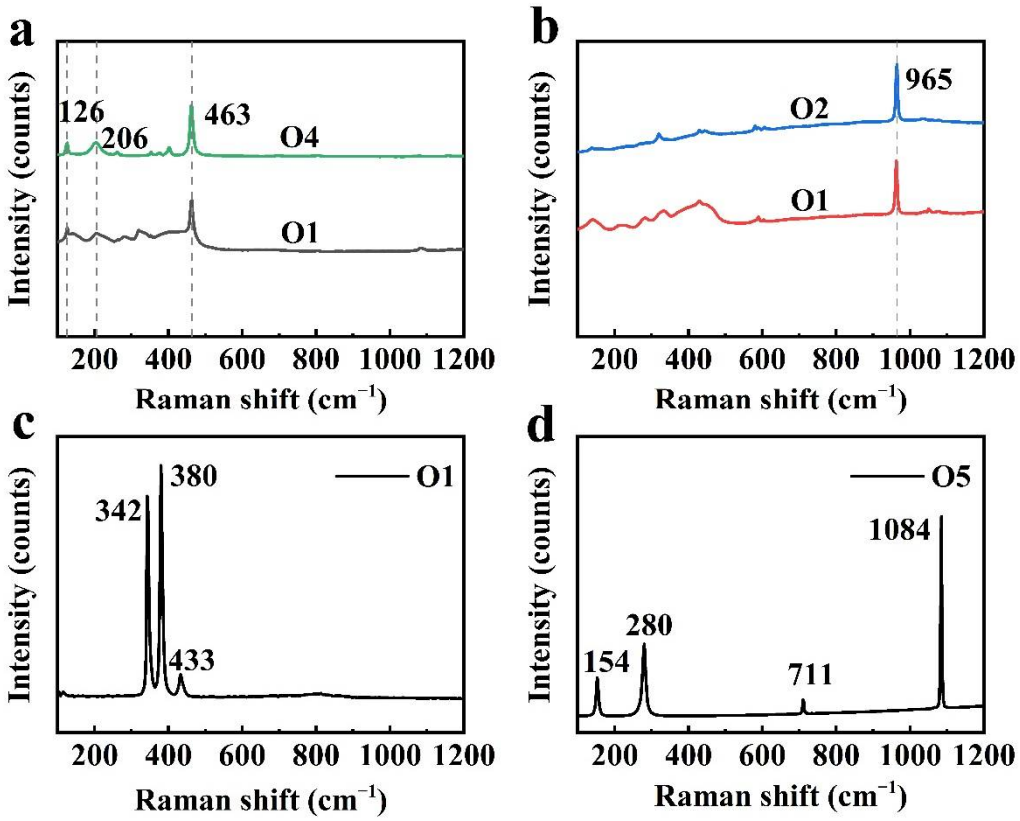

Figure 7. The Raman microprobe spectra for various minerals in the ore samples. (**a**) Quartz; (**b**) apatite; (**c**) pyrite; (**d**) calcite.

Table 1. The mode assignments of different minerals.

Minerals	Raman Shift, cm^{-1}	Assignment	References
Quartz	126 206, 463	E(t) + E(1) modes A_1 mode	[41,42]
Apatite	965	V_1 mode	[43,44]
Pyrite	342 380 433	E_g mode A_g mode T_g mode	[45,46]
Calcite	154, 280 711 1084	Ca–O V_4 mode V_1 mode	[47]

4.2.3. UV–Visible Spectra

The UV–Visible spectra for the purple fluorites are quite similar (Figure 8a–d). The wide and strong bands in the range of 564 to 585 nm, which appear in different samples, correspond to Ca colloids. After long-term irradiation of radioelement in fluorite or surrounding rock, F^- will lose electrons, and Ca^{2+} captures these electrons to form Ca colloids. The Ca colloids absorb visible light at 560–580 nm, which makes the fluorite appear purple [48,49].

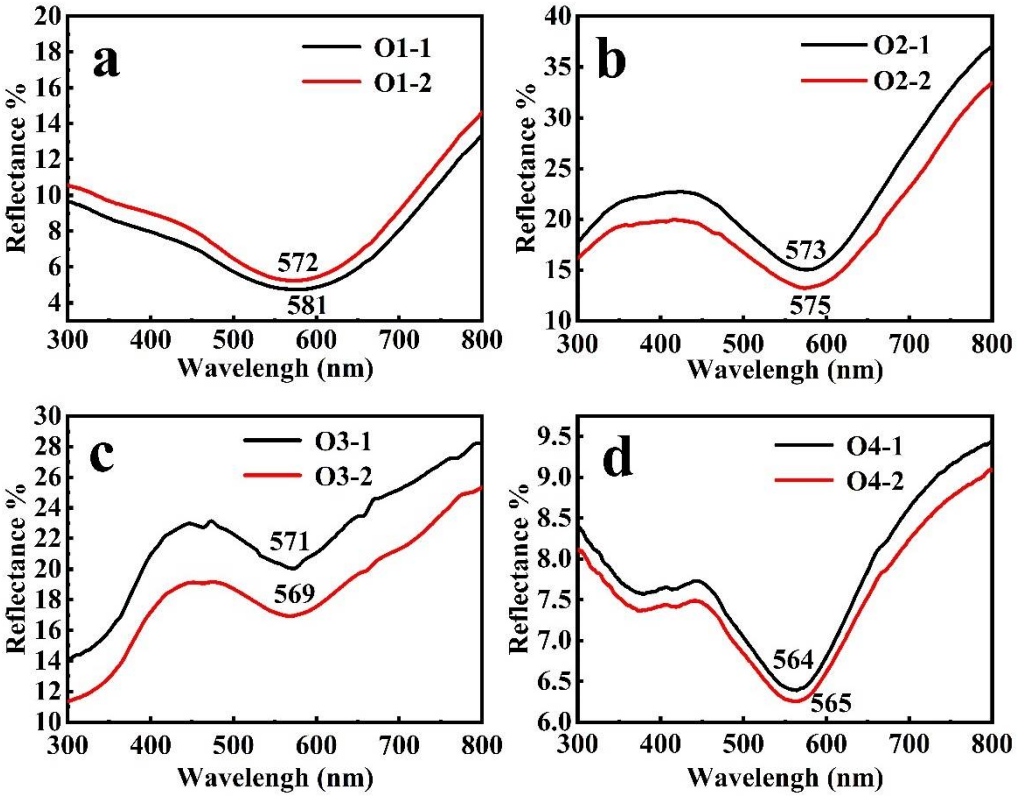

Figure 8. UV–Vis spectra for the ore samples. (**a**) O1; (**b**) O2; (**c**) O3; (**d**) O4.

4.3. Characteristics of Fluid Inclusions

The abundant small fluid inclusions in the Nanlishu fluorite are elliptical (Figure 9a), drop shaped (Figure 9b), fasciculate, or triangular, mainly distributed in groups or in isolation. They have two (liquid–vapor) phases and the primary fluid inclusions are 3–5 μm in size.

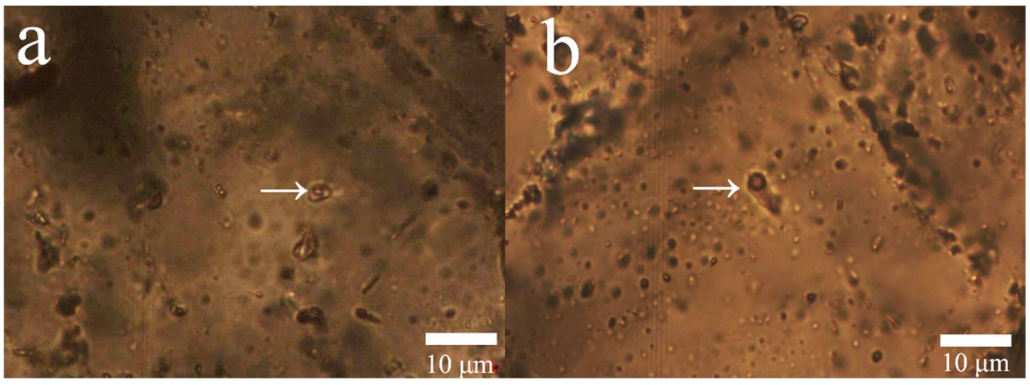

Figure 9. Fluid inclusions in Nanlishu fluorite. (**a**) Elliptical fluid inclusion; (**b**) drop-shaped fluid inclusion. →, The fluid inclusions in the Nanlishu fluorite.

4.3.1. Micro Thermometry Results

A total of 34 fluid inclusions within fluorite from O2 were analyzed for homogenization and freezing temperatures (Table A1). The homogenization temperatures vary from 116–179 °C and the salinity ranges from 0.35 to 4.03 wt% NaCl equiv. Their distributions are relatively even, with no obvious peaks or phases (Figure 10a,b). Density is calculated using the standard formula after Liu and varies from 0.90–1.00 g/cm^3 [50].

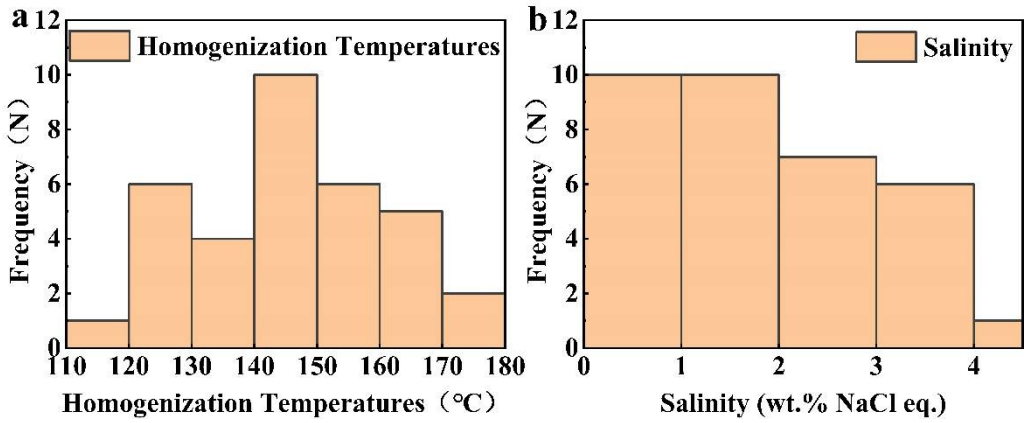

Figure 10. The frequency histograms for homogenization temperature and salinity of the fluid inclusions. (**a**) Homogenization temperature; (**b**) salinity.

4.3.2. Fluid Inclusion Composition

The Raman spectra of individual fluid inclusions are presented in Figure 11. The liquid–vapor phase composition of fluid inclusions in the Nanlishu fluorite is mainly H_2O, which produces bands at 3050–3736 cm^{-1} related to the O–H stretching modes (Figure 11a–f). A small quantity of CO_2 was detected in one fluid inclusion; the two bands at 1283 and 1386 cm^{-1} in the vapor phase and two bands at 1281 and 1380 cm^{-1} in the liquid phase are all assigned to the CO_2 symmetrical stretching modes (Figure 11g,h) [51].

4.4. REE Geochemistry

4.4.1. REE Characteristics

In combination with PLM observation, O1, O2, and O3, which represent the ore in different mineralization stages, were selected to discuss the REE characteristics of the Nanlishu fluorite. The REE characteristics of Nanlishu fluorite are listed in Table 2. The total rare earth element (∑REE, excluding Y) contents of samples O1–O3 ranged from 8.072 to 27.230 ppm, which are relatively lower than those of fluorite from other regions in China [52–66]. The light/heavy REE ratio (LREE/HREE) varies from 0.971 to 1.513, which is not obviously enriched in LREEs or HREEs. There are almost no anomalies in δEu (1.010–1.074) and δCe (0.893–1.048). The ionic radii of Eu^{3+} and Ce^{3+} are closer to that of Ca^{2+} than other rare earth elements, and they more easily enter the lattice in isomorphism. Compared with the fluorite from other origins in China, Nanlishu fluorite has lower ∑REE content, no obvious enrichment in LREEs or HREEs, and no anomalies in δEu or δCe (Table A2) [52–66].

4.4.2. Chondrite-Normalized REE Patterns

An REE/chondrite normalized distribution pattern is constructed (Figure 12), and the chondrite values are taken from Sun [67]. The distribution curves of O1 and O2 have similar characteristics but are different from O3. Combined with PLM observation, it is suggested that O1 and O2 formed from the early ore-forming fluid, and O3 is formed from the late ore-forming fluid. A small quantity of late ore-forming fluid precipitated and crystallized along the crystallographic planes of the early fluorite (Figure 4c).

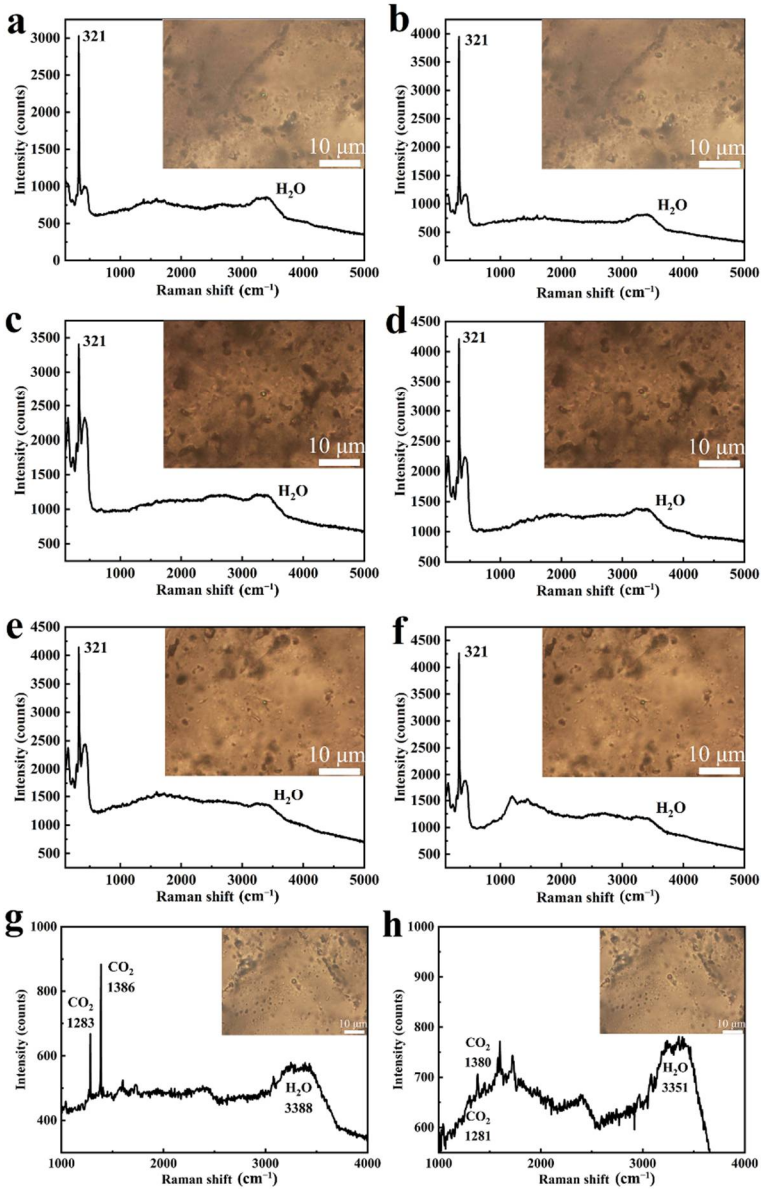

Figure 11. Raman microprobe spectra for liquid–vapor phase fluid inclusions. (**a**–**f**) Spectra for liquid–vapor phase with H_2O as the main composition; (**g**,**h**) spectra for liquid–vapor phase with CO_2 as the main composition.

Table 2. Rare earth element contents of ore samples (ppm).

Samples	O1	O2	O3
La	0.870	2.410	1.800
Ce	1.630	5.140	5.160
Pr	0.230	0.710	0.810
Nd	1.040	3.370	4.270
Sm	0.360	1.210	1.890
Eu	0.168	0.580	0.760
Gd	0.697	2.253	2.804
Tb	0.139	0.431	0.475
Dy	1.017	3.349	2.805

Table 2. *Cont.*

Samples	O1	O2	O3
Ho	0.228	0.847	0.540
Er	0.730	2.910	1.470
Tm	0.111	0.442	0.194
Yb	0.739	3.116	1.238
Lu	0.113	0.462	0.181
Y	8.480	31.230	17.590
∑REE	8.072	27.230	24.397
∑LREE	4.298	13.420	14.690
∑HREE	3.774	13.810	9.707
LREE/HREE	1.139	0.971	1.513
δEu	1.025	1.074	1.010
δCe	0.893	0.963	1.048

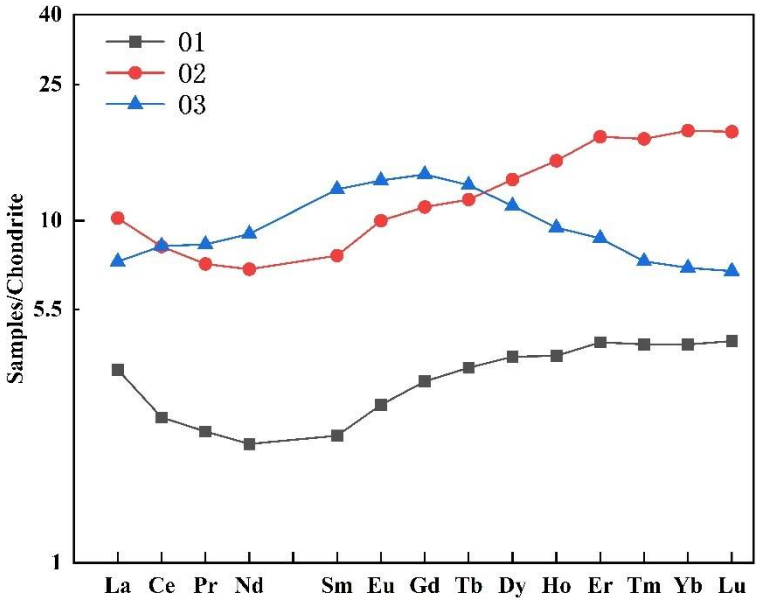

Figure 12. REE/chondrite normalized distribution pattern of ore samples.

4.4.3. The Tb/Ca–Tb/La Diagram

Based on the analysis of more than 150 fluorite samples from various regions of the world, Möller proposed a Tb/Ca–Tb/La diagram, which divided fluorite deposit genesis into three types: pegmatitic, hydrothermal, and sedimentary [68]. When calculating the Tb/Ca atomic ratio in this work, n(Ca) adopts the theoretical value (51.3328%) in CaF_2 (Table A3). Taking the Tb/La atomic ratio in Nanlishu fluorite as the abscissa and the Tb/Ca atomic ratio as the ordinate, the data were mainly projected in the hydrothermal genesis area, similar to the fluorite in different deposits in China (Figure 13) [53–66].

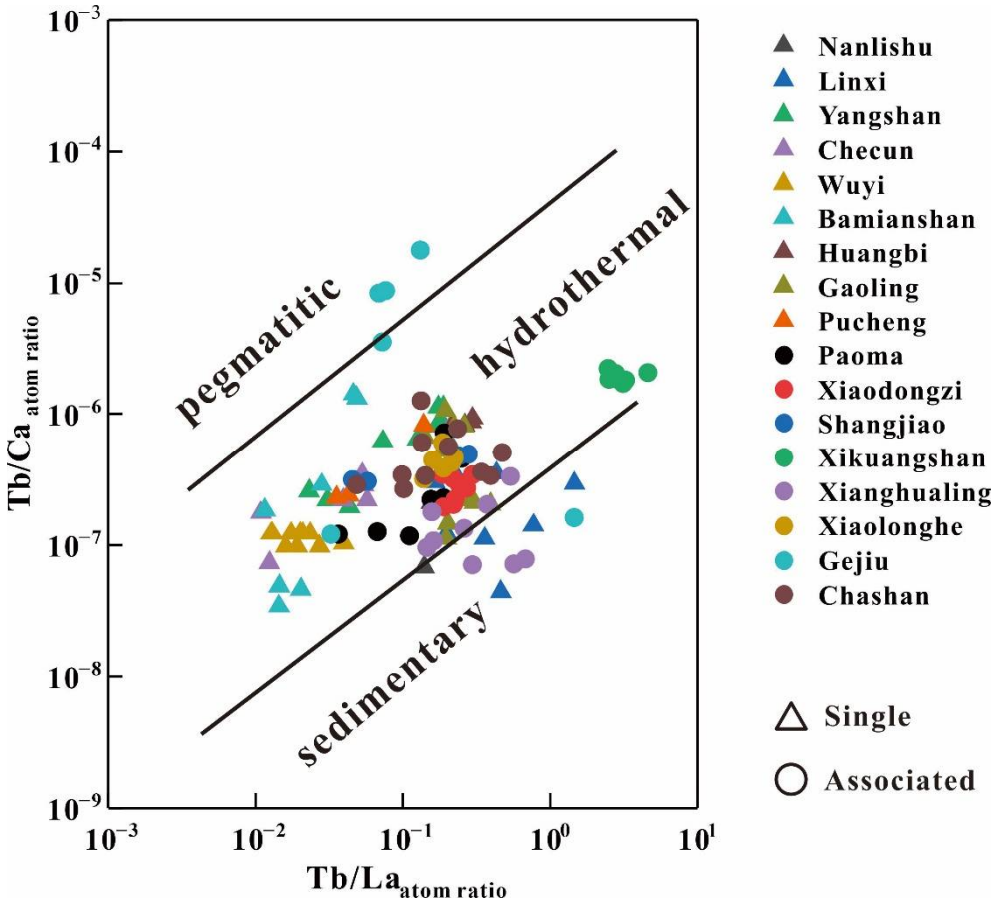

Figure 13. The Tb/Ca–Tb/La diagram of fluorite in different deposits in China [53–66].

5. Discussion

5.1. Origin of Ore-Forming Fluids

Previous studies indicated that the magmatic rocks in the Nanlishu mining area were mostly intrusive rocks, among which the quartz syenite porphyry is the direct source rock of fluorite mineralization. Magmatism provides a significant heat source and hydrothermal fluid containing fluorine, encouraging fluorite mineralization. The surrounding rock provides abundant calcium for fluorite mineralization. Therefore, it is concluded that the Nanlishu fluorite ore-forming fluid is a late magmatic hydrothermal solution (intrusion of the quartz syenite porphyry) [22].

Based on previous studies, this work summarizes the characteristics of fluid inclusions in fluorite from hydrothermal filling type and associated type deposits in China (Table A4) [23–33]. The maximum ore-forming temperatures of fluorite with magmatic water as the main ore-forming fluid exceeds 200 °C. The ore-forming temperatures of fluorite with meteoric water as the main ore-forming fluid are often lower than 220 °C (Table A4). The salinity of magmatic water is generally higher than that of meteoric water. The homogenization temperatures of fluid inclusions in the Nanlishu fluorite vary from 116 to 179 °C and do not fit with magmatic water or late magmatic hydrothermal solution as the ore-forming fluid. The salinity ranges from 0.35 to 4.03 wt% NaCl equiv, which corresponds to the range of meteoric water. The density varies from 0.90 to 1.00 g/cm^3 and is distributed evenly. Therefore, the ore-forming fluids are derived from heated meteoric water characterized by low temperature, low salinity, and low density.

In addition, the mineral compositions of late magmatic hydrothermal deposits are usually oxides, sulfides, and oxysalts, and the metallogenic elements are complex. In this work, the Nanlishu fluorite ore rock is composed mainly of fluorite with minor amounts of quartz, pyrite, and apatite and trace amounts of calcite, which is different from late

magmatic hydrothermal fluorite deposits. The surrounding rock, which is silicified and pyritized, is characteristic of meteoric water alteration [23]. Therefore, the conclusion that the Nanlishu fluorite ore-forming fluid was a late magmatic hydrothermal solution is invalid.

5.2. Origin of the Deposit

The mechanisms of fluorite precipitation are mainly changes in temperature, pressure, or pH of ore-forming fluids rich in Ca and F; mixing of two brines of different chemical compositions, and water/rock reaction of F-rich ore-forming fluid metasomatizing the surrounding calcareous rocks [69]. In addition to quartz syenite porphyry, the surrounding rock of the ore bodies is mainly tuff with argillaceous limestone and siliceous rock, among which the limestone can provide a large quantity of Ca for fluorite mineralization. F could be from the biotite in the quartz syenite porphyry or leached and extracted from the Carboniferous strata during the ascent and migration of meteoric water. Therefore, water/rock reaction is suggested as the main mechanism for Nanlishu fluorite precipitation.

In combination with PLM observation and chondrite-normalized REE patterns, the mineralization of fluorite can be divided into two stages: the early fluorite is small-grained and dark in color, while the late fluorite is large-grained and light in color. The early fluorite was frequently filled with vein-type quartz and sociated with quartz, pyrite, and apatite, suggesting that the early fluorite has undergone quartz–sulfide mineralization stage, which could be related to the late magmatism of the quartz syenite porphyry intrusion.

The developed fractures and folds in the area were conducive to fluorite mineralization. The NW-oriented secondary faults influenced by the Lishugou fault were the main faults controlling the ore belt and ore bodies. Meteoric water infiltrated into the deep strata due to gravity and sedimentary compaction and was heated by geothermal warming and magmatism (intrusion of the quartz syenite porphyry), absorbing F from the strata through convection to form F-bearing fluid. As a result of late tectonism, the F-bearing fluid rose from the deep strata to the shallow surface along the faults. F in the surrounding rock was continuously leached and extracted and migrated in the fluid in the form of ion complexes [19,24]. After reaching the surface, the ore-forming fluid reacted with the surrounding rocks, replacing the calcium in the limestone, enriching in metallogenic elements, and finally crystallizing into ore (Figure 14). The vein-type and lens-type ore bodies are strictly controlled by the fault belt. The Nanlishu fluorite deposit is a fault-controlled, low-temperature hydrothermal, fracture-filling deposit.

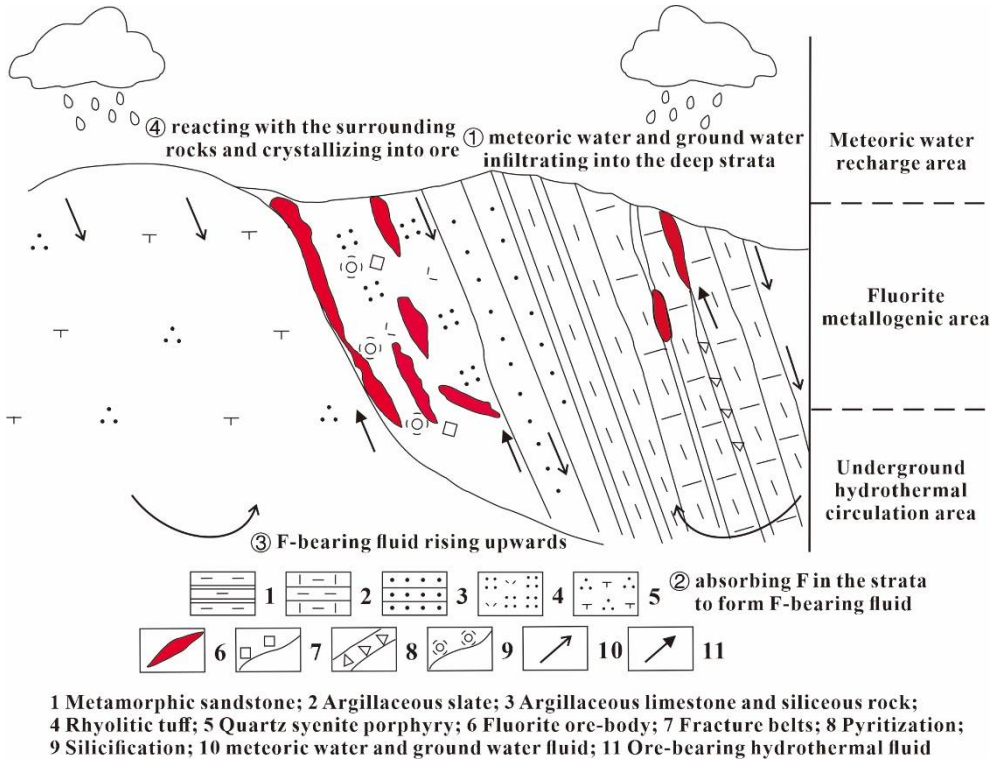

Figure 14. Metallogenic model of the Nanlishu fluorite deposit (after Yan, 2019) [22].

6. Conclusions

In this research, mineral composition, mineral structure, spectral characteristics, fluid inclusion, and rare earth element geochemistry were conducted to discuss the constraints on the metallogenic mechanism of the Nanlishu fluorite deposit. More methods to measure the origin of ore-forming fluid directly, such as isotopic analysis, should be undertaken in future research.

The Nanlishu fluorite ore rock is composed mainly of fluorite with minor amounts of quartz, pyrite, and apatite, and trace amounts of calcite. The early fluorite was small-grained and dark in color, while the late fluorite was large-grained and light in color. The purple color of the fluorite is caused by the Ca colloids.

The homogenization temperatures of fluid inclusions vary from 116 to 179 °C, the salinity ranges from 0.35 to 4.03 wt% NaCl equiv, and the density varies from 0.90 to 1.00 g/cm^3. Ore-forming fluids were derived from heated meteoric water characterized by low temperature, low salinity, and low density.

The metallogenic mechanism of the Nanlishu fluorite deposit is water/rock reaction, which is related to the meteoric water and the surrounding limestone. Dark-colored fluorite formed in the early ore-forming fluids, and light-colored fluorite formed in late ore-forming fluids. The ore bodies are vein type and lens type, strictly controlled by the fault belt. The Nanlishu fluorite deposit is a fault-control, low-temperature hydrothermal, fracture-filling type deposit.

Author Contributions: Conceptualization, X.Y. and F.B.; methodology, X.Y. and F.B.; software, X.Y.; validation, X.Y.; formal analysis, X.Y.; investigation, X.Y.; resources, F.B.; data curation, X.Y.; writing—original draft preparation, X.Y.; writing—review and editing, F.B.; visualization, X.Y.; supervision, F.B.; project administration, F.B.; funding acquisition, F.B. All authors have read and agreed to the published version of the manuscript.

Funding: This research received no external funding.

Data Availability Statement: Not applicable.

Acknowledgments: Thanks to the Experimental Teaching Center of Jewelry and Mineral Materials, China University of Geosciences, Beijing for the experimental equipment.

Conflicts of Interest: The authors declare no conflict of interest.

Appendix A

Table A1. Microthermometry results of primary fluid inclusions in Nanlishu fluorite.

Host Mineral	Size (μm)	Steam Volume (%)	Tm (°C)	Tm, Ice (°C)	Salinity (wt% NaCl Equiv)	Density (g/cm^3)
Fluorite	5	10	128	−2.3	3.87	0.97
Fluorite	5	10	141	−2.1	3.55	0.95
Fluorite	4	30	136	−1.1	1.91	0.95
Fluorite	2	10	120	−0.7	1.22	0.96
Fluorite	4	20	168	−0.4	0.70	0.91
Fluorite	4	30	161	−1.9	3.23	0.93
Fluorite	3	20	174	−0.7	1.22	0.91
Fluorite	3	25	148	−1.3	2.24	0.94
Fluorite	4	40	155	−0.4	0.70	0.92
Fluorite	3	35	143	−0.2	0.35	0.93
Fluorite	3	20	148	−1.5	2.57	0.94
Fluorite	4	20	142	−0.8	1.40	0.94
Fluorite	3	30	179	−0.3	0.53	0.90
Fluorite	2	10	152	−1.1	1.91	0.93
Fluorite	6	40	168	−1.9	3.23	0.93
Fluorite	4	15	125	−1.2	2.07	0.96
Fluorite	3	30	124	−1.1	1.91	0.96
Fluorite	4	25	129	−1.6	2.74	0.96
Fluorite	5	15	129	−1.1	1.91	0.96
Fluorite	5	20	130	−0.7	1.22	0.95
Fluorite	5	20	156	−0.4	0.70	0.92
Fluorite	4	25	153	−0.4	0.70	0.93
Fluorite	3	35	136	−1.4	2.41	0.95
Fluorite	3	20	141	−0.2	0.35	0.94
Fluorite	5	15	154	−1.5	2.57	0.94
Fluorite	4	20	134	−0.5	0.88	0.95
Fluorite	4	15	145	−1.1	1.91	0.94
Fluorite	4	10	116	−0.4	0.70	0.96
Fluorite	4	10	143	−0.3	0.53	0.94
Fluorite	8	20	153	−2.4	4.03	0.95
Fluorite	5	15	169	−1.0	1.74	0.92
Fluorite	6	40	140	−1.3	2.24	0.95
Fluorite	5	20	162	−2.1	3.55	0.93
Fluorite	5	30	145	−2.0	3.39	0.95

Tm, homogenization temperature; Tm, ice, final ice-melting temperature.

Table A2. Rare earth elements contents of fluorite in different deposits in China [52–66].

Deposits	Deposit Type	Main Minerals in the Deposit	REE (ppm)	LREE/HREE	δEu	δCe
Nanlishu	Single	Fl, Qtz, Py	8.072–27.230	0.971–1.513	1.010–1.074	0.893–1.048
Stunt Qagan Obo	Single	Fl, Qtz, Cal, Py	10.080–207.000	0.640–2.960	0.540–2.120	0.270–0.680
Shuitou	Single	Fl, Qtz, Kln	4.370–158.000	0.240–1.800	0.570–1.600	0.810–0.980
Yangshan	Single	Fl, Qtz	41.910–147.250	0.710–2.210	0.630–0.700	0.840–0.940
Checun	Single	Fl, Qtz, Kln, Chl	17.100–239.200	1.080–1.780	0.320–1.950	0.960–2.190
Wuyi	Single	Fl, Qtz, Kln, Ser	11.800–192.280	0.260–4.260	0.360–0.910	0.680–0.960
Bamianshan	Single	Fl, Cal, Qtz	3.620–38.400	8.160–17.190	0.450–1.300	0.890–1.140
Huangbi	Single	Fl, Cal, Qtz	75.240–84.240	0.880–1.110	0.430–0.460	0.990–1.000
Gaoling	Single	Fl, Qtz, Cal, Sti, Py	11.400–105.000	0.790–1.650	0.910–1.200	0.510–0.900
Pucheng	Single	Fl, Qtz, Cal, Py, Ser	12.220–154.440	1.100–4.670	0.550–1.050	0.730–0.950
Paoma	Associated	Gn, Sph, Py, Fl, Qtz,	9.230–60.850	0.920–5.300	0.800–2.940	0.580–1.000
Xiaodongzi	Associated	Gn, Sph, Qtz, Fl	17.140–68.340	1.280–5.060	1.310–2.010	0.740–4.510
Shangjiao	Associated	Ur, Fl, Qtz	41.870–68.970	0.950–4.330	0.630–0.650	1.120–1.230
Xikuangshan	Associated	Sti, Qtz, Cal, Fl	100.090–139.380	0.813–1.190	0.770–0.830	0.920–1.060
Xianghualing	Associated	Cst, Ars, Sh, Dol, Fl	298.950–3135.420	0.400–3.330	0.020–0.110	0.940–2.060
Xiaolonghe	Associated	Cst, Mu, Bit, Toz, Fl	12.860–1420.800	0.240–2.540	0.200–0.430	0.890–0.980
Gejiu	Associated	Py, Ars, Cp Qtz, Fl	7.000–1277.000	0.502–3.263	0.010–0.190	0.440–1.050
Chashan	Associated	Sti, Qtz, Fl	4.030–77.530	1.530–2.840	1.480–2.940	0.760–0.870

Single, fluorite is the main mineral in these deposits; Associated, fluorite is the associated mineral in these deposits. Fl, fluorite; Qtz, quartz; Py, pyrite; Ap, apatite; Cal, calcite; Chl, chlorite; Ser, sericite; Sti, stibnite; Gn, galena; Spn, sphalerite; Ur, Uraninite; Cst, cassiterite; Ars, arsenopyrite; Sh, scheelite; Dol, dolomite; Mu, muscovite; Bit, biotite; Toz, Topaz; Cp, chalcopyrite.

Table A3. Tb/La and Tb/Ca atomic ratios of ore samples.

Samples	O1	O2	O3
La	0.870	2.410	1.800
Tb	0.139	0.431	0.475
n(Tb/La)	0.140	0.156	0.231
n(Tb/Ca)	0.068	0.211	0.232

Table A4. Characteristics of fluid inclusions in different fluorite deposits in China [23–33].

Deposit	Deposit Type	Ore-Forming Temperature (°C)	Salinity (wt% NaCl Equiv)	Ore-Forming Fluid
Nanlishu	Single	116–179	0.35–8.41	Meteoric water
Linxi	Single	140–220	0.4–2.8	Meteoric water
Wuyi	Single	84–130	1.7–5.2	Meteoric water
Huangshuangling	Single	150–200	0.18–3.06	Meteoric water
Bamianshan	Single	120–250	0.18–4.18	Meteoric water, magmatic water, metamorphic water
Bancang	Single	93–186	0.35–9.28	Meteoric water
Nankeng	Single	150–160	0.5–4.0	Meteoric water
Huitan	Single	114–160	0.88–13.82	Meteoric water
Chizhuyuan	Associated	250–300	2–9.21	Magmatic water, meteoric water
Xihuashan	Associated	140–295	1.4–7.7	Magmatic water, meteoric water
Huangshaping	Associated	135–313	0.88–19.13	Magmatic water, meteoric water
Beilu	Associated	90–288	0.18–13.45	Magmatic water, metamorphic water, meteoric water

Single, fluorite is the main mineral in these deposits; Associated, fluorite is the associated mineral in these deposits.

References

1. Bill, H. Origin of the coloration of yellow fluorites: The O^{3-} center structure and dynamical aspects. *J. Chem. Phys.* **1982**, *76*, 219–224. [CrossRef]
2. Gaft, M.; Waychunas, G.A.; Rossman, G.R.; Nagli, L.; Panczer, G.; Cheskis, D.; Raichlin, Y. Red photoluminescence and purple color of naturally irradiated fluorite. *Phys. Chem. Miner.* **2020**, *47*, 45–56. [CrossRef]
3. Aoki, T.; Garvie, L.A.J.; Rez, P. Observation of color center peaks in calcium fluoride. *Ultramicroscopy* **2015**, *153*, 40–44. [CrossRef] [PubMed]
4. Gu, H.; Ma, D.; Chen, W.; Zhu, R.; Li, Y.; Li, Y. Electrolytic coloration and spectral properties of natural fluorite crystals containing oxygen impurities. *Spectrochim. Acta Part A Mol. Biomol. Spectrosc.* **2011**, *82*, 327–331. [CrossRef] [PubMed]
5. Bill, H.; Calas, G. Color centers, associated rare-earth ions and the origin of coloration in natural fluorites. *Phys. Chem. Miner.* **1978**, *3*, 117–131. [CrossRef]
6. Dill, H.G.; Weber, B. Variation of color, structure and morphology of fluorite and the origin of the hydrothermal F-Ba deposits at Nabburg-Wolsendorf, SE Germany. *Neues Jahrb. Mineral. Abh.* **2010**, *187*, 113–132. [CrossRef]
7. Kempe, U.; Plötze, M.; Brachmann, A.; Böttcher, R. Stabilisation of divalent rare earth elements in natural fluorite. *Miner. Petrol.* **2002**, *76*, 213–234. [CrossRef]
8. Mackenzie, K.J.D.; Green, J.M. The cause of coloration in Derbyshire Blue John banded fluorite and other blue banded fluorites. *Mineral. Mag.* **1971**, *38*, 459–470. [CrossRef]
9. Braithwaite, R.S.W.; Flowers, W.T.; Haszeldine, R.N.; Russell, M. The cause of the colour of Blue John and other purple fluorites. *Mineral. Mag.* **1973**, *39*, 401–411. [CrossRef]
10. Galwey, A.K.; Jones, K.A.; Reed, R.; Dollimore, D. The blue coloration in banded fluorite (Blue John) from Castleton, Derbyshire, England. *Mineral. Mag.* **1979**, *43*, 243–250. [CrossRef]
11. Sasmaz, A.; Kryuchenko, N.; Zhovinsky, E.; Suyarko, V.; Konakci, N.; Akgul, B. Major, trace and rare earth element (REE) geochemistry of different coloredfluorites in the Bobrynets region, Ukraine. *Ore Geol. Rev.* **2018**, *102*, 338–350. [CrossRef]
12. Mondillo, N.; Boni, M.; Balassone, G.; Spoleto, S.; Stellato, F.; Marino, A.; Santoro, L.; Spratt, J. Rare earth elements (REE)–Minerals in the Silius fluorite vein system (Sardinia, Italy). *Ore Geol. Rev.* **2016**, *74*, 211–224. [CrossRef]
13. Öztürk, H.; Altuncu, S.; Hanilçi, N.; Kasapçı, C.; Goodenough, K.M. Rare earth element-bearing fluorite deposits of Turkey: An overview. *Ore Geol. Rev.* **2019**, *105*, 423–444. [CrossRef]
14. Eppinger, R.G.; Closs, L.G. Variation of trace elements and rare earth elements in fluorite; a possible tool for exploration. *Econ. Geol.* **1990**, *85*, 1896–1907. [CrossRef]
15. Duan, Z.; Jiang, S.; Su, H.; Zhu, X.; Zou, T.; Cheng, X.; Jiang, S.; Su, H.; Zhu, X.; Zou, T.; et al. Trace and rare earth elements, and Sr isotopic compositions of fluorite from the Shihuiyao rare metal deposit, inner Mongolia: Implication for its origin. *Minerals* **2020**, *10*, 882. [CrossRef]
16. Haschke, S.; Gutzmer, J.; Wohlgemuth-Ueberwasser, C.; Kraemer, D.; Burisch, M. The Niederschlag fluorite-(barite) deposit, Erzgebirge/Germany—a fluid inclusion and trace element study. *Miner. Depos.* **2021**, *56*, 1071–1086. [CrossRef]
17. Kraemer, D.; Viehmann, S.; Banks, D.; Sumoondur, A.; Koeberl, C.; Bau, M. Regional variations in fluid formation and metal sources in MVT mineralization in the Pennine Orefield, UK: Implications from rare earth element and yttrium distribution, Sr-Nd isotopes and fluid inclusion compositions of hydrothermal vein fluorites. *Ore Geol. Rev.* **2019**, *107*, 960–972. [CrossRef]
18. Li, X.; Wang, G.; Mao, W.; Wang, C.; Xiao, R.; Wang, M. Fluid inclusions, muscovite Ar–Ar age, and fluorite trace elements at the Baiyanghe volcanic Be–U–Mo deposit, Xinjiang, northwest China: Implication for its genesis. *Ore Geol. Rev.* **2015**, *64*, 387–399. [CrossRef]
19. Pei, Q.; Zhang, S.; Santosh, M.; Cao, H.; Zhang, W.; Hu, X.; Wang, L. Geochronology, geochemistry, fluid inclusion and C, O and Hf isotope compositions of the Shuitou fluorite deposit, Inner Mongolia, China. *Ore Geol. Rev.* **2017**, *83*, 174–190. [CrossRef]
20. Hein, U.F.; Lüders, V.; Dulski, P. The fluorite vein mineralization of the southern Alps: Combined application of fluid inclusions and rare earth element (REE) distribution. *Mineral. Mag.* **1990**, *54*, 323–333. [CrossRef]
21. Sasmaz, A.; Yavuz, F. REE geochemistry and fluid-inclusion studies of fluorite deposits from the Yaylagozu area (Yildizeli-Sivas) in Central Turkey. *Neues Jahrb. Mineral. Abh.* **2008**, *183*, 215–226. [CrossRef]
22. Yang, L. Geological characteristics and genesis of the Nanlishu fluorite deposit in Mingcheng Town, Panshi City, Jilin Province. *Jilin Geol.* **2019**, *38*, 49–51. (In Chinese)
23. Zhang, S.; Cao, H.; Zheng, G.; Ma, Y.; Fang, Y.; Zou, H. Characteristics of ore-forming fluids and mineralization processes of the Shuitou fluorite deposit in Linxi, Inner Mongolia Autonomous region. *Earth Sci. Front.* **2014**, *21*, 31–40. (In Chinese)
24. Zeng, Z.; Cao, H.; Gao, F.; Gao, Y.; Zou, H.; Li, D. Fluid inclusion study of fluorite deposits in Linxi region, Inner Mongolia. *Geochimica* **2013**, *42*, 73–81. (In Chinese)
25. Ma, J. Study on mineral inclusions of fluorite deposits in Wuyi, Zhejiang province. *Resour. Surv. Environ.* **1990**, *11*, 13–24. (In Chinese)
26. Lu, W.; Yang, S.; Zhang, P. Isotopic investigation of Huangshuangling Fluorite deposit in Sheng county, Zejiang. *J. Chengdu Coll. Geol.* **1991**, *18*, 103–111. (In Chinese)
27. Wang, X.; Wang, S.; Yuan, Y.; Li, Y. Characteristics of geological and metallogenic fluids on Bancang fluorite mine in Dawu, Hubei. *Miner. Explor.* **2019**, *10*, 2256–2260. (In Chinese)

28. Wen, H.; Wang, J. The characteristics of fluorite inclusions and genesis of Nankeng Fluorite deposit. *Mineral. Petrol.* **1992**, *12*, 74–79. (In Chinese)
29. Li, Z. Geological characteristics and genesis of Huitan fluorite deposit in Jianyang city, Fujian province. *Geol. Fujian* **2021**, *40*, 13–23. (In Chinese)
30. Wang, L.; Ni, P.; Dai, B.; Li, W.; Pan, J.; Cui, J.; Gao, Y. Fluid inclusion study of the ore-bearing stockwork greisen at Shizhuyuan W-Sn-Mo-Bi deposit, Hunan. *J. Nanjing Univ.* **2020**, *56*, 653–665. (In Chinese)
31. Huang, H.; Chang, H.; Tan, J.; Li, F.; Zhang, C.; Zhou, Y. Contrasting infrared microthermometry study of fluid inclusions in coexisting quartz, wolframite and other minerals: A case study of Xihuashan quartz-vein tungsten deposit, China. *Acta Petrol. Sin.* **2015**, *31*, 925–940. (In Chinese)
32. Huang, C.; Li, X.; Wang, L.; Liu, F. Fluid inclusion study of the Huangshaping polymetallic deposit, Hunan Province, South China. *Acta Petrol. Sin.* **2013**, *29*, 4232–4244. (In Chinese)
33. Suo, Z.; Wang, S.; Yu, Z.; Li, Y.; Yuan, Y.; Wang, X. Hydrogen, oxygen, lead and sulfur isotopic and geochemical characteristics of fluorite deposits in the North Dabie Mountains. *Miner. Resour. Geol.* **2020**, *34*, 41–47. (In Chinese)
34. Campbell, S.; Dusseault, M.; Xu, B.; Michaelian, K.H.; Poduska, K.M. Photoacoustic detection of weakabsorption bands in infrared spectraof calcite. *Appl. Spectrosc.* **2021**, *75*, 795–801. [CrossRef]
35. Zhang, M.; Moxon, T. Infrared absorption spectroscopy of SiO_2–moganite. *Am. Mineral.* **2014**, *99*, 671–680. [CrossRef]
36. Kučírková, A.; Navrátil, K. Interpretation of infrared transmittance spectra of SiO_2 thin films. *Appl. Spectrosc.* **1994**, *48*, 113–120. [CrossRef]
37. Jin, R.; Hu, S.; Tan, Y. Preparation of ultrafine SiO_2 powder from rice husk and properties of its infrared spectrum. *J. Meas. Sci. Instrum.* **2011**, *2*, 262–269. [CrossRef]
38. Čermáková, Z.; Bezdička, P.; Němec, I.; Hradilová, J.; Šrein, V.; Blažekf, J.; Hradila, D. Naturally irradiated fluorite as a historic violetpigment: Raman spectroscopic and X-ray diffraction study. *J. Raman Spectrosc.* **2015**, *46*, 236–243. [CrossRef]
39. Keramidas, V.G.; White, W.B. Raman spectra of oxides with the fluorite structure. *J. Chem. Phys.* **1973**, *59*, 1561–1562. [CrossRef]
40. Srivastava, R.; Lauer, H.V.; Chase, L.L.; Bron, W.E. Raman frequencies of fluorite crystals. *Phys. Lett. A* **1971**, *36*, 333–334. [CrossRef]
41. Sato, R.K.; McMillan, P.F. An infrared and Raman study of the isotopic species of α-quartz. *J. Phys. Chem.* **1987**, *91*, 3494–3498. [CrossRef]
42. Zu, E.; Li, S.; Zou, Y.; Zhao, X.; Sun, Y.; Lin, Y.; Li, H. Study of natural and synthetic quartz by Raman spectra. *Key Eng. Mater.* **2011**, *492*, 341–344. [CrossRef]
43. Xu, B.; Kou, G.; Etschmann, B.; Liu, D.; Brugger, J. Spectroscopic, Raman, EMPA, Micro-XRF and Micro-XANES analyses of sulphur concentration and oxidation state of natural apatite crystals. *Crystals* **2020**, *10*, 1032. [CrossRef]
44. Wang, M.; Qian, R.; Bao, M.; Gu, C.; Zhu, P. Raman, FT-IR and XRD study of bovine bone mineral and carbonated apatites with different carbonate levels. *Mater. Lett.* **2018**, *210*, 203–206. [CrossRef]
45. Chen, C.; Li, H.; Yuan, Y.; Zhang, M.; Shuai, S.; Wan, J. Raman spectroscopic studies of pyrite at high pressure and high temperature. *Minerals* **2022**, *12*, 332. [CrossRef]
46. Zhang, H.; Qian, G.; Cai, Y.; Gibson, C.; Pring, A. Crystal chemistry of arsenian pyrites: A Raman spectroscopic study. *Am. Mineral.* **2022**, *107*, 274–281. [CrossRef]
47. Ishida, K.; Hawthorne, F.C. Raman characterization of synthetic magnesian calcites. *Am. Mineral.* **2016**, *101*, 2525–2538. [CrossRef]
48. McLaughlan, S.D.; Evans, H.W. Production of colloidal calcium by electron irradiation of CaF_2 crystals. *Phys. Status Solidi B* **1968**, *27*, 695–700. [CrossRef]
49. LeBret, J.B.; Norton, M.G.; Dickinson, J.T.; Cramer, L.P. Colloid formation and laser-induced bleaching in fluorite. *Appl. Phys. Lett.* **2005**, *85*, 4382–4384. [CrossRef]
50. Liu, B.; Duan, G. The density and isochoric formulae for NaCl–H_2O fluid inclusions (salinity ≤25 wt%) and their applications. *Acta Mineral. Sin.* **1987**, *7*, 345–352. (In Chinese)
51. Frezzotti, M.L.; Tecce, F.; Casagli, A. Raman spectroscopy for fluid inclusion analysis. *J. Geochem. Explor.* **2012**, *112*, 1–20. [CrossRef]
52. Xu, D.; Nie, F.; Qian, M.; Liu, Y.; Yun, F.; Zhang, W. REE geochemistry and genesis of Sumochagan Obo superlarge fluorite deposit. *Miner. Depos.* **2009**, *28*, 29–41. (In Chinese)
53. Cao, H.; Zhang, S. REE geochemistry of fluorite from Linxi fluorite deposit and its geological implications, Inner Mongolia Autonomous Region. *Geochimica* **2014**, *43*, 131–140. (In Chinese)
54. Feng, S.; Wang, J.; Liu, Y.; Liang, X.; Huang, L.; Zhang, Z.; Xiao, H. Geochemical characteristics, and indicative significance of rareearth elements in Yangshan fluorite deposit in western Henan province. *Chin. Rare Earths* **2020**, *41*, 50–58. (In Chinese)
55. Dong, W.; Pang, X.; Si, Y.; Liang, Z.; Li, W. REE geological characteristics of Checun fluorite deposit in Song county, Henan province. *J. Chin. Soc. Rare Earths* **2020**, *38*, 706–714. (In Chinese)
56. Xia, X.; Han, Y.; Lian, W.; Yuan, C.; Xu, S.; Yan, F.; Liang, Z. Genesis discussion and REE geochemistry characters in Bamianshan fluorite deposit in Zhejiang province. *Geol. Chem. Miner.* **2009**, *31*, 193–200. (In Chinese)
57. Huang, H.; Luo, P.; Chang, S.; Zhang, J.; Wang, C. Characteristics of rare earth elements and the source of mineralization of fluorite deposit in Huangbi, Jiangxi Province. *Miner. Resour. Geol.* **2018**, *32*, 641–654. (In Chinese)

58. Jin, S.; Chen, J.; Dai, D.; Yang, D.; Zhou, J.; He, X. Geochemical characteristics of trace elements and REE in the Gaoling fluorite deposit, Southwest Guizhou, China. *Acta Mineral. Sin.* **2018**, *38*, 684–692. (In Chinese)
59. Zhu, L.; Jin, S.; Wang, C.; Shang, P.; Gao, L.; Wang, Z. Geochemistry characteristic and genesis of surrounding rock and ore Pucheng Fluorite Deposit district, Fujiang province. *Acta Petrogr. Mineral.* **2021**, *40*, 923–938. (In Chinese)
60. Wu, Y.; Zhang, C.; Tian, G. REE geochemistry of fluorite from Paoma lead-zinc deposit in Sichuan province, China and its geological implications. China. *Acta Mineral. Sin.* **2013**, *33*, 295–301. (In Chinese)
61. Luo, L.; Tan, H.; Hu, J.; Xie, H.; Zhang, W. REE geochemistry of the Xiaodongzi fluorite deposit in Butuo. *Acta Geol. Sichuan* **2020**, *40*, 45–50. (In Chinese)
62. Wu, D.; Pan, J.; Xia, F.; Huang, G.; Zhang, F.; Lan, J.; Qi, J.; Liu, Y. Characteristics and source significance of rare earth elements geochemistry of fluorite from Shangjiao uranium deposit in southern Jiangxi Province. *Chin. Rare. Earths* **2019**, *40*, 14–26. (In Chinese)
63. Lin, F.; Peng, J.; Hu, A.; Deng, M. Geochemical study of REE in fluorite from Xikuangshan antimony deposit, central Hunan Province, China. *Acta Mineral. Sin.* **2015**, *35*, 214–220. (In Chinese)
64. Cao, H.; Zhang, W.; Pei, Q.; Zhang, S.; Zheng, G. Trace element geochemistry of fluorite and calcite from the Xiaolonghe tin deposits and Lailishan tin deposits in western Yunnan, China. *Bull. Mineral. Petrol. Geochem.* **2016**, *36*, 925–935. (In Chinese)
65. Peng, Q.; Jiang, X.; Li, C.; Fan, Z.; Wei, C.; Chen, Y.; Xie, X.; Yu, H. Geochemical characteristics of fluorites from the Xi'ao altered granite type Cu-Sn polymetallic deposit in Gejiu, Yunnan Province and their geological significance. *Miner. Depos.* **2021**, *40*, 1182–1198. (In Chinese)
66. Nie, A. REE geochemistry and origin of fluorite from Chashan antimony deposit, Guangxi. *Acta Mineral. Sin.* **1998**, *18*, 250–253. (In Chinese)
67. Sun, S.-S.; McDonough, W.F. Chemical and isotopic systematics of oceanic basalts: Implications for mantle composition and processes. *Geol. Soc. Lond. Spec. Publ.* **1989**, *42*, 313–345. [CrossRef]
68. Möller, P.; Parekh, P.P.; Schneider, H.-J. The application of Tb/Ca-Tb/La abundance ratios to problems of fluorspar genesis. *Miner. Depos.* **1976**, *11*, 111–116. [CrossRef]
69. Richardson, C.K.; Holland, H.D. Fluorite deposition in hydrothermal systems. Geochimicaica et Cosmochimica. *Geochim. Cosmochim. Acta* **1979**, *43*, 1327–1335. [CrossRef]